IOP Conf. Series: Journal of Physics: Conf. Series **1037** (2018) 072023 doi:10.1088/1742-6596/1037/7/072023

Quantification of the axial induction exerted by utility-scale wind turbines by coupling LiDAR measurements and RANS simulations

Giacomo Valerio Iungo, Stefano Letizia and Lu Zhan

Wind Fluids and Experiments (WindFluX) Laboratory, Mechanical Engineering Department, The University of Texas at Dallas, Richardson, 75080 Texas, USA

E-mail: valerio.iungo@utdallas.edu

Abstract. The axial induction exerted by utility-scale wind turbines for different operative and atmospheric conditions is estimated by coupling ground-based LiDAR measurements and RANS simulations. The LiDAR data are thoroughly post-processed in order to average the wake velocity fields by using as common reference frame their respective wake directions and the turbine hub location. The various LiDAR scans are clustered according to their incoming wind speed at hub height and atmospheric stability regime, namely Bulk Richardson number. Time-averaged velocity fields are then calculated as ensemble averages of the scans belonging to the same cluster. The LiDAR measurements are coupled with RANS simulations in order to estimate the rotor axial induction for each cluster of the LiDAR data. First, a control volume analysis of the streamwise momentum is applied to the time-averaged LiDAR velocity fields to obtain an initial estimate of the axial induction over the rotor disk. The calculated thrust force is imposed as forcing of an axisymmetric RANS simulation in order to estimate pressure, radial velocity and momentum fluxes. The latter are combined with the LiDAR streamwise velocity field in order to refine the estimate of the rotor axial induction through the control volume approach. This process is repeated iteratively until achieving convergence on the rotor axial induction while minimizing difference between LiDAR and RANS streamwise velocity fields. This procedure allows to single out the reduction in thrust load while the blade pitch angle is increased transitioning from region 2 to 3 of the power curve. Furthermore, an enhanced thrust force is observed for a fixed incoming wind speed and transitioning from stable to convective stability regimes. The presented technique is proposed as a data-driven alternative to the blade element momentum theory typically used with current actuator disk models in order to quantify rotor aerodynamic thrust for different operative and atmospheric conditions.

1. Introduction

Quantification of the aerodynamic forcing exerted by utility-scale wind turbines on the atmospheric boundary layer (ABL) for different turbine settings and atmospheric stability conditions is one of the greatest challenges to overcome in order to achieve accurate predictions of wind turbine wakes and power capture.

Numerical simulations of wind turbine wakes are typically performed by means of actuator line or disk models [1-7], which rely on tabulated data of the blade geometry and aerodynamic coefficients for the various airfoils composing the blades. These parameters, coupled with the evaluation of the relative wind speed along the turbine blades, allow predicting the rotor aerodynamic forces. Blade geometry and airfoil characteristics are typically proprietary data and

not publicly available for real wind turbines, which justifies the wide use of turbine archetypes to perform wake investigations, such as the 5-MW NREL wind turbine [8]. Even when turbine data are available, the aerodynamic forcing of a real turbine rotor can differ significantly from the predictions obtained from the blade element momentum theory due to the 3D turbulent nature of the incoming ABL flow and to the boundary layer evolving over the blades, which is typically not simulated with the existing actuator line/disk models. The divergence of actual aerodynamic performance of turbine blades during real operations with respect to the design condition is systematically proven by the variability of turbine power curves for different atmospheric stability regimes and relative locations of the turbines within a wind farm [9-11].

Effects of power capture exerted by wind turbines on the ABL consist in the generation of wakes, which are flow regions located downstream of each turbine characterized by a reduced wind speed and enhanced wind turbulence. Moving downstream, the momentum fluxes make the wake velocity field gradually recovering to the incoming ABL profile. It has been documented experimentally [9, 12] and through numerical simulations [13], that the enhanced turbulence intensity connected with convective stability conditions promotes wake recovery reducing wake interactions and, in turn, power under-performance of downstream wind turbines [9].

Wind turbine wakes can extend downstream to the turbine location for distances longer than ten rotor diameters [9]. Therefore, probing wakes generated by utility-scale wind turbines requires measurement techniques capable to cover such large volumes, while providing adequate spatio-temporal resolution to characterize wake turbulent flows. A very promising remote sensing technique for probing wakes generated by utility-scale wind turbines is light detection and ranging (LiDAR), allowing measurements of ABL flows [14-16] and wind turbine wakes [17-19] through a variety of scanning strategies ranging from 1D fast scans to characterize wind turbulence [20, 21] to volumetric scans for characterizations of 3D ABL flows and wakes [12].

In this paper, to achieve enhanced accuracy in the quantification of the aerodynamic forcing exerted by utility-scale wind turbines for different atmospheric stability conditions and turbine settings, the axial induction at the rotor disk is quantified by coupling LiDAR wake measurements with RANS simulations. LiDAR measurements, collected for an onshore wind farm located in North Texas, are analyzed through a control volume analysis of the streamwise momentum in order to provide an estimate of the thrust force distribution over the rotor disk. The latter is injected in a RANS solver as forcing on the incoming freestream. The RANS simulations provide estimates for pressure, radial velocity and shear stress flux, which are then leveraged within the control volume analysis in order to refine the estimate of the axial induction over the rotor disk. This iterative procedure is stopped when convergence on the axial induction is achieved and difference between LiDAR and RANS streamwise velocity fields is minimized. This study enables investigating the variability of the rotor thrust force for different incoming wind speed and atmospheric stability conditions.

The remainder of the paper is organized as follows. The wind farm and the experimental setup is described in Sect. 2. The main features of the RANS solver are reported in Sect. 3, while the post-processing of the LiDAR data for calculating the time-averaged wake velocity fields is summarized in Sect. 4. Subsequently, the LiDAR data are coupled with RANS simulations in Sect. 5 to estimate the turbine axial induction. Concluding remarks are reported in Sect. 6.

2. Site and Experimental Setup

A field campaign was performed for an onshore wind farm located in North Texas consisting of four rows of identical 2.3-MW wind turbines extended along the east-west direction. These turbines have a rotor diameter, D, of 108 m and hub height of 80 m. The measurement campaign was conducted through various phases between August 2015 and March 2017. Meteorological data, collected for the entire duration of the experiment from a met-tower, were provided as ten-minute averages and standard deviation of wind speed, wind direction, temperature, humidity

and barometric pressure, at heights of 36 m, 60 m, and 80 m.

Supervisory control and data acquisition (SCADA) data were provided for each turbine as ten-minute averages and standard deviation of wind speed, power output, rotor rotational velocity, blade pitch and rotor yaw angle. These data were used to calculate power curves for the various wind turbines according to the IEC standard, as well as to assess parameters retrieved from the LiDAR measurements [9].

The wind velocity around and within the turbine array was measured with a Windcube 200S manufactured by Leosphere, which is a scanning Doppler wind LiDAR embedded in a mobile station to allow easy deployment, control, data collection and monitoring of the instrument [9]. This LiDAR is characterized by a typical scanning range of 4 km, while a range gate of 50 m and accumulation time of 500 ms were used.

Single-wake plan position indicator (PPI) scans were performed to maximize spatio-temporal resolution of the wake measurements. Main constraints in the selection of the scan parameters consisted in achieving a carrier-to-noise ratio (CNR) higher than -25 dB throughout the range of interest, and collecting measurements at hub height within the downstream range 1-3 D with at least five measurement points in the transverse direction within the wake. The sampling period for a single PPI scan was always smaller than 10 s. LiDAR wake measurements were performed only for wind turbines at the southernmost row for southerly wind directions in order to avoid wake interactions for the present study.

3. RANS solver

The turbulent axisymmetric wake generated by a rotor disk exposed to a uniform incoming wind speed, U_∞, is simulated through the Reynolds-averaged Navier-Stokes (RANS) equations for incompressible flows:

$$\begin{cases} \frac{\partial U_x}{\partial x} + \frac{1}{r}\frac{\partial}{\partial r}(rU_r) = 0 \\ U_x\frac{\partial U_x}{\partial x} + U_r\frac{\partial U_x}{\partial r} = -F_t - \frac{\partial p}{\partial x} + \left(\frac{1}{Re} + \nu_T\right)\left[\frac{\partial^2 U_x}{\partial x^2} + \frac{1}{r}\frac{\partial}{\partial r}\left(r\frac{\partial U_x}{\partial r}\right)\right] \\ U_x\frac{\partial U_r}{\partial x} + U_r\frac{\partial U_r}{\partial r} = -\frac{\partial p}{\partial r} + \left(\frac{1}{Re} + \nu_T\right)\left[\frac{\partial^2 U_r}{\partial x^2} + \frac{1}{r}\frac{\partial}{\partial r}\left(r\frac{\partial U_r}{\partial r}\right) - \frac{U_r}{r^2}\right] \end{cases} \quad (1)$$

where U_x and U_r are the time-averaged streamwise and radial velocities, respectively, made non-dimensional with U_∞. The pressure, p, is made non-dimensional with ρU_∞^2, where ρ is the air density. The Reynolds number, Re, is defined with U_∞ and the rotor diameter of the wind turbine, D. F_t is the thrust force exerted by the rotor disk and ν_T is a uniform turbulent eddy viscosity. It is noteworthy that in Eq. 1, the swirling velocity induced by the turbine is neglected, which is clearly a good approximation for the far-wake region. Through a preliminary analysis, not shown here for the sake of brevity, it was found that adding a modeled swirling velocity in the control volume analysis does not affect noticeably the estimates of the rotor axial induction.

The numerical domain consists of a circular cylinder with axis at hub height parallel the wake direction. After a grid sensitivity analysis, the RANS computational domain was set with the inlet boundary at a distance of 5 D upstream to the rotor disk, while the outlet is at a downstream distance of 8 D. The radius of the numerical domain is 2 D. Free-stress boundary condition is imposed at the lateral boundary. At the symmetry axis, radial velocity is zeroed, likewise for the gradients of the streamwise velocity and pressure. At the outlet, a non-homogeneous Neumann condition is applied by imposing the velocity gradients in the streamwise direction equal to their respective values at the adjacent upstream grid points. The streamwise velocity field at the inlet is implemented as Dirichlet condition with null radial velocity.

Eq. 1 together with the boundary conditions are discretized via a Chebyshev spectral collocation method implemented in Matlab [3]. To ensure numerical stability, the flow field is calculated over a rectangular grid made of $N_x = 65$ and $N_r = 40$ points in the streamwise and

radial directions, respectively, while pressure is calculated on a staggered grid of $(N_x-2)\times(N_r-2)$ grid points. Within the rotor area, the grid has 20 nodes in the radial direction. The resulting non-linear system is solved by means of the Newton iterative algorithm with a convergence threshold equal to 10^{-8} for the L_2-norm of the residual of the RANS solution.

4. Post-processing of LiDAR data and time-averaged wake velocity fields

Each wake velocity field is represented with respect to a reference frame whose origin is the hub location of the specific turbine under investigation and x-direction pointing downwards in the wake direction. The latter is obtained as linear fitting of the minimum velocity deficits estimated at various downstream locations through the Gaussian fitting in the transverse direction of the wake velocity profiles. Each LiDAR sample is reported in a reference frame where x is the downstream distance from the turbine rotor, while r is the radial distance from the wake direction with sign to indicate the two sides of the wake. For more details on the LiDAR measurements and data post-processing see [22].

From the LiDAR radial velocity, V_r, an approximation for the horizontal wind speed, U_{eq}, is obtained as follows:

$$U_{eq} = V_r/cos\phi/cos(\theta - \theta_w) \tag{2}$$

where ϕ and θ are the elevation and azimuthal angles, respectively, of the LiDAR laser beam, while θ_w is the wake direction for the specific PPI scan.

The LiDAR velocity field is then made non-dimensional through the incoming ABL profile, which is also estimated through the LiDAR measurements [22]. This procedure allows to directly compare the various wake velocity fields avoiding the typical distortion induced by the wind shear. Furthermore, the long-wave meandering-like oscillations are filtered out in order to achieve a time-averaged velocity field analogous to that predicted through the RANS simulations. This filtering process is performed by aligning the wake centers at various downstream locations with the mean wake direction, θ_w.

The various PPI scans are then clustered as a function of the incoming wind speed at hub height while keeping a sufficient number of LiDAR scans for each cluster in order to achieve statistical convergence in the data analysis. The experimental power curve for the turbines under investigation and the blade pitch angle are reported in Figs. 1a and b, respectively. The used bin edges of the incoming wind speed normalized with the turbine rated speed are 0.35, 0.65, 0.8, 0.9, 1 and 1.15, while the number of PPI scans for each cluster are reported in Figs. 1d over a total number of about 11,000 PPI scans.

Each cluster defined through the incoming wind speed is then split in three sub-clusters based on atmospheric stability regime. Bulk Richardson number, Ri_B, calculated from the available meteorological data is used to further cluster the LiDAR data among convective ($Ri_B <$ -0.0024), neutral (-0.0024$\leq Ri_B \leq$ 0.0011) and stable ($Ri_B >$ 0.0011) conditions [22].

The wake velocity fields obtained through PPI scans belonging to the same cluster are then ensemble-averaged in order to provide an estimate for the time-averaged wake velocity fields. The ensemble average is performed through the Barnes scheme [23]. Accuracy in the estimate of the average velocity fields is monitored by rejecting all the values with an error on the mean larger than 1% and interpolating the mean velocity at that location with a bi-harmonic algorithm. The obtained average velocity fields are reported for each cluster in Fig. 2. The black dashed lines delimit areas with data rejected through the quality control process and interpolated.

The typical faster wake recovery occurring during convective conditions compared to neutral and stable conditions [9, 12] is clearly detected through the average velocity fields. Furthermore, a gradually reducing velocity deficit is observed with increasing incoming wind speed. This wake feature is certainly connected with the transition from operations of region 2 of the power curve (for incoming wind speeds between cut-in and rated) and region 3 (for incoming wind speeds

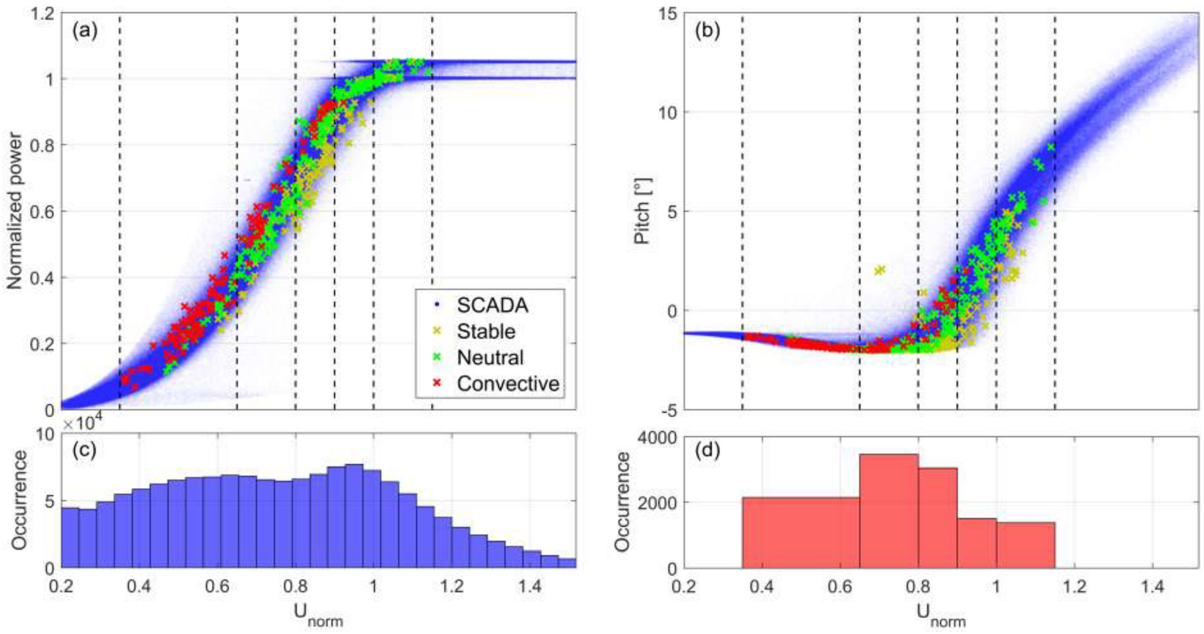

Figure 1. SCADA data: a) Normalized power; b) blade pitch angle; c) number of SCADA data for each 0.5-m/s wide bin; d) number of PPI scans for each cluster.

between rated and cut-off), for which an increased blade pitch angle leads to a reduction of the thrust coefficient of the turbine rotor.

It is noteworthy that the wake velocity profiles for high thrust coefficient conditions (low incoming wind speed) show an evident non-symmetry with respect to the wake center. This wake feature, which can be better appreciated from the mean velocity profiles at x/D=3.25 reported in Fig. 3, might represent a source of inaccuracy for our current axisymmetric approach for the analysis of the LiDAR data and RANS simulations. However, this observed wake asymmetry seems to be reasonable and due to the combination of high vertical wind shear of the incoming wind, which is typical for stable atmospheric conditions, and a strong wake shear [24].

5. Estimate of axial induction by coupling LiDAR data and RANS simulations

The mean velocity field calculated from the LiDAR data is first leveraged to estimate the optimal turbulent-eddy viscosity, ν_T, for each cluster. Preliminary RANS simulations have been performed by using as inlet the average velocity, U_{eq}, measured at x/D=3.25, which is a downstream location where the pressure can be considered practically recovered to ambient pressure and the turbulent fluxes being the major component in the momentum equation [6, 7].

The ν_T has been optimally tuned by using as objective functional the minimization of the mean absolute percentage error (MAPE) between the LiDAR and RANS streamwise velocity fields over the far-wake region with x/D >3.25. The optimization problem has been carried out in Matlab with the command fmincon and using the sequential quadratic programming. The optimally-tuned ν_T is reported in Fig. 4 showing an increase of ν_T transitioning from stable to neutral and convective stability regimes. This trend is associated with the general increase of the incoming wind turbulence intensity due to the different stability regimes. Furthermore, a reduction of ν_T is observed with increased incoming wind speed at hub height. This suggests that ν_T also encompasses effects of the wake-generated turbulence, which is generally proportional to the wake velocity shear, thus it is reduced with higher incoming wind speeds (Fig. 3).

The final value of the objective functional for the optimization of the ν_T, namely the MAPE, is reported in Fig. 4b. A larger error is typically achieved for stable conditions due to the less axisymmetry of the wake velocity fields, as mentioned above (Fig. 3).

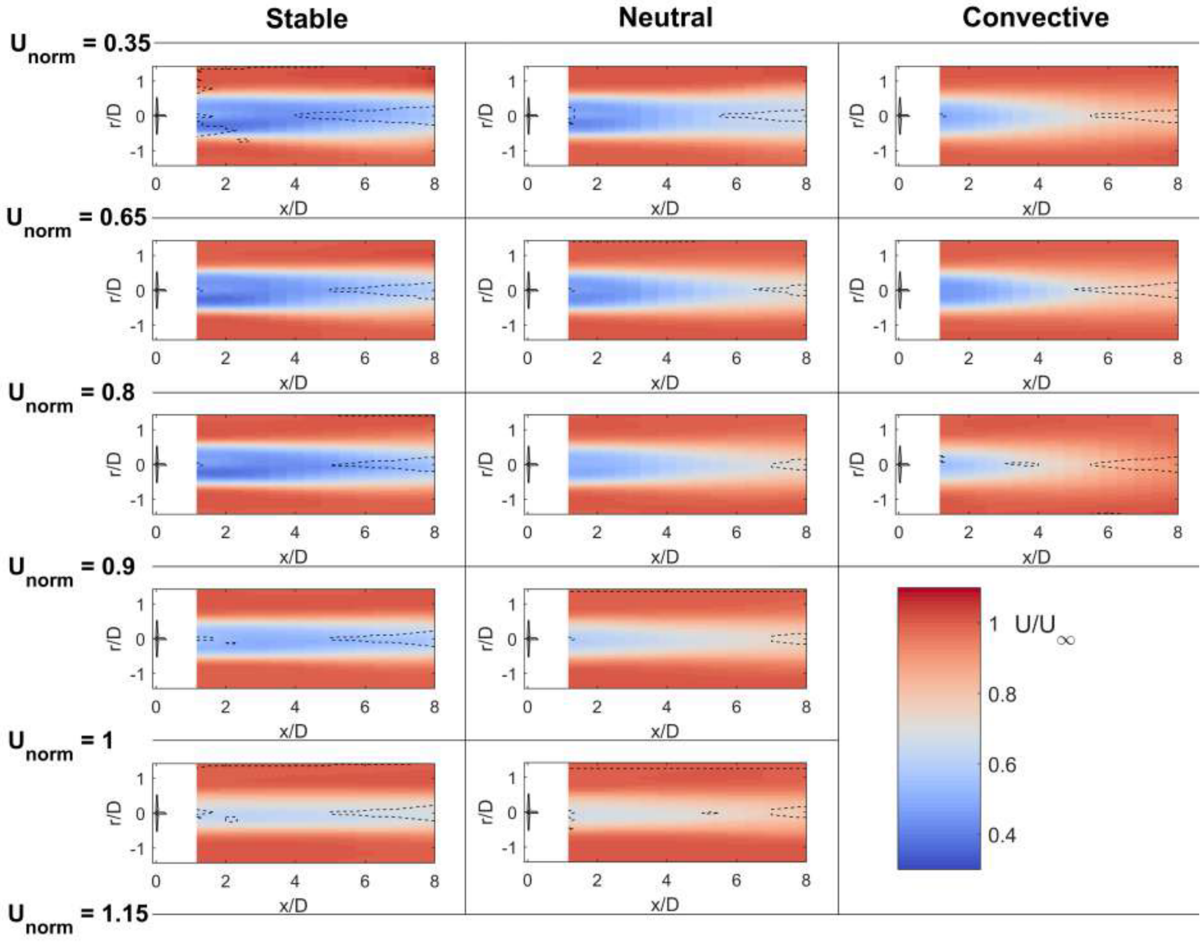

Figure 2. Mean streamwise equivalent velocity field, U_{eq}, calculated for each cluster based on incoming wind speed at hub height and atmospheric stability regime.

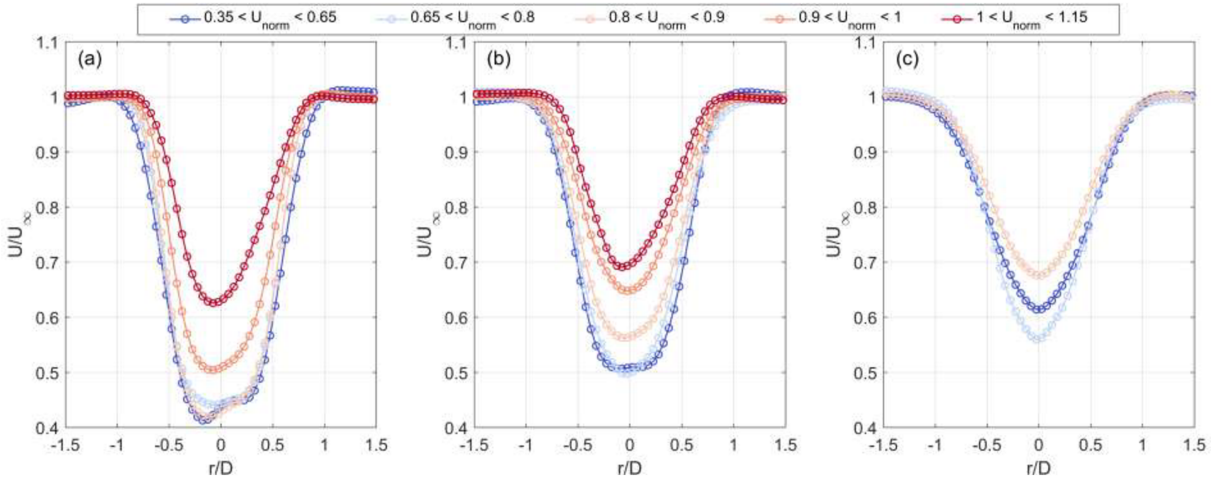

Figure 3. Mean streamwise equivalent velocity, U_{eq}, calculated at the location x/D=3.25 for various incoming wind speed and atmospheric stability: a) stable; b) neutral; c) convective.

The axial induction exerted by the blades is estimated through a control volume analysis of the streamwise momentum. The adopted control volumes are concentric cylinders with ring cross-sections (except for the innermost one having circular cross-section) and axes coincident

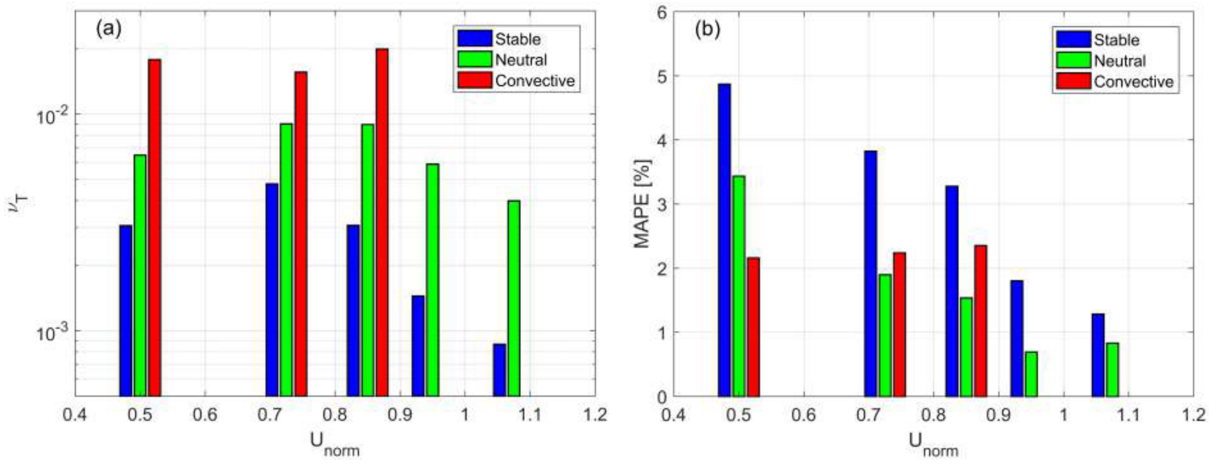

Figure 4. Optimal tuning of the turbulent-eddy viscosity, ν_T, for the various LiDAR clusters and atmospheric stability regimes: a) ν_T; b) mean absolute percentage error.

with the x-direction. The upstream base of the cylinder is at a position x_0 =-5 D, which is far enough from the turbine rotor in order to be considered as immersed in the freestream, while the downstream base is at $\overline{x}$ =1.15 D, which is the downstream location closest to the turbine rotor for which LiDAR data are available. For a control volume with inner and outer radii equal to R_1 and R_2, respectively, the momentum budget can be written as:

$$-\pi U_\infty^2(R_2^2-R_1^2)+2\pi\int_{R_1}^{R_2}U_x^2(\overline{x})rdr-2\pi R_1\int_{x_0}^{\overline{x}}U_x(R_1)U_r(R_1)dx+2\pi R_2\int_{x_0}^{\overline{x}}U_x(R_2)U_r(R_2)dx=$$
$$=-\tfrac{2\pi}{\rho}\int_{R_1}^{R_2}F_t rdr-\tfrac{2\pi R_1}{\rho}\int_{x_0}^{\overline{x}}\tau_{xr}(R_1)dx+\tfrac{2\pi R_2}{\rho}\int_{x_0}^{\overline{x}}\tau_{xr}(R_2)dx+\tfrac{2\pi}{\rho}\int_{R_1}^{R_2}(-p(\overline{x})+\tau_{xx}(\overline{x}))rdr \quad (3)$$

where F_t is the axial force exerted by the rotor within the selected control volume, which is the unknown of the equation, and R_2-R_1=0.01 D. The shear stresses are calculated as:

$$\begin{aligned}\tau_{xx}&=2\rho U_\infty D(1/Re+\nu_T)\tfrac{\partial U_x}{\partial x}\\ \tau_{xr}&=\rho U_\infty D(1/Re+\nu_T)(\tfrac{\partial U_x}{\partial r}+\tfrac{\partial U_r}{\partial x})\end{aligned} \quad (4)$$

As first attempt to estimate F_t, Eq. 3 is applied for the various control volumes by neglecting p, U_r and τ, while U_x at $\overline{x}$ =1.15 D is the mean velocity measured by the LiDAR for the specific cluster under investigation. The calculated thrust force is then used as a forcing for the first RANS simulation.

The data obtained from the first RANS simulation and the LiDAR data at $\overline{x}$ =1.15 D are then injected in Eq. 3 for a new estimate of the thrust force, which is then used in the RANS solver for a new simulation. This procedure is performed iteratively with a threshold equal to 1% on the MAPE between LiDAR and RANS velocity at $\overline{x}$ =1.15 D. Spurious thrust force may appear for some radial locations beyond the blade tip due to uncertainty of the turbulence closure and post-processing of the LiDAR data. However, this is disregarded for the thrust estimates because leading to differences in the velocity field with MAPE lower than 5%.

An example of the application of the iterative procedure to estimate thrust force distribution and relative wake velocity profile at $\overline{x}$ =1.15 D is reported in Fig. 5 for the cluster with $0.65 < U_{norm} < 0.8$ and neutral stability regime. For this case, the initial thrust force estimated by only using the LiDAR data is gradually modified in order to maximize the agreement in the velocity profile with the LiDAR data. The thrust force is gradually reduced at the middle span of the blade, while the load is increased towards the tip in order to widen the wake, as measured by the LiDAR. Convergence is typically achieved with less than 20 iterations.

The thrust distribution calculated for the various clusters is reported in Fig. 6. For low incoming wind speeds, the peak aerodynamic load is typically located towards the blade tip.

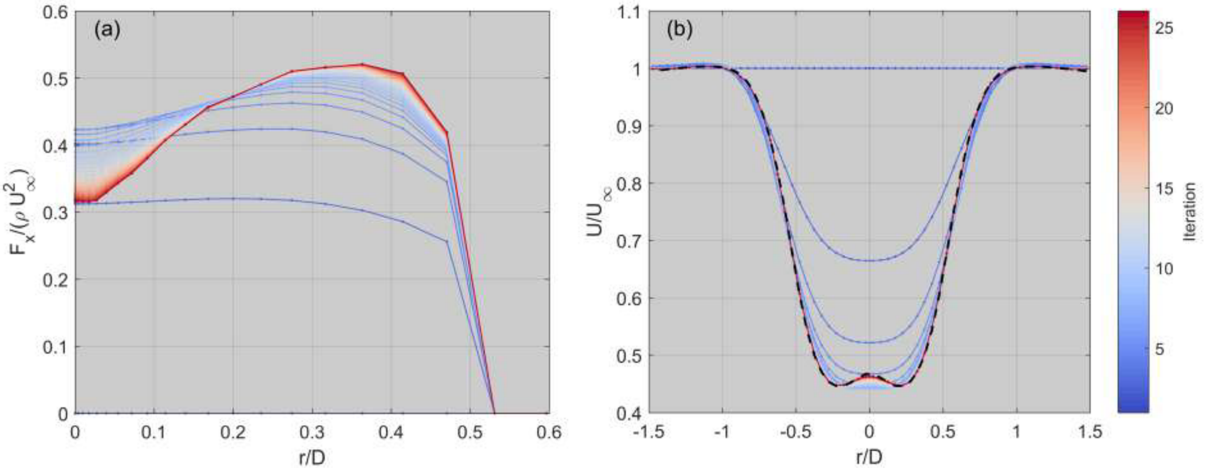

Figure 5. Iterative estimation of the local thrust force for the cluster with $0.65 < U_{norm} < 0.80$ under neutral atmospheric conditions: a) thrust force; b) RANS streamwise velocity at $\overline{x}$ =1.15 D (respective LiDAR data reported with dashed black line).

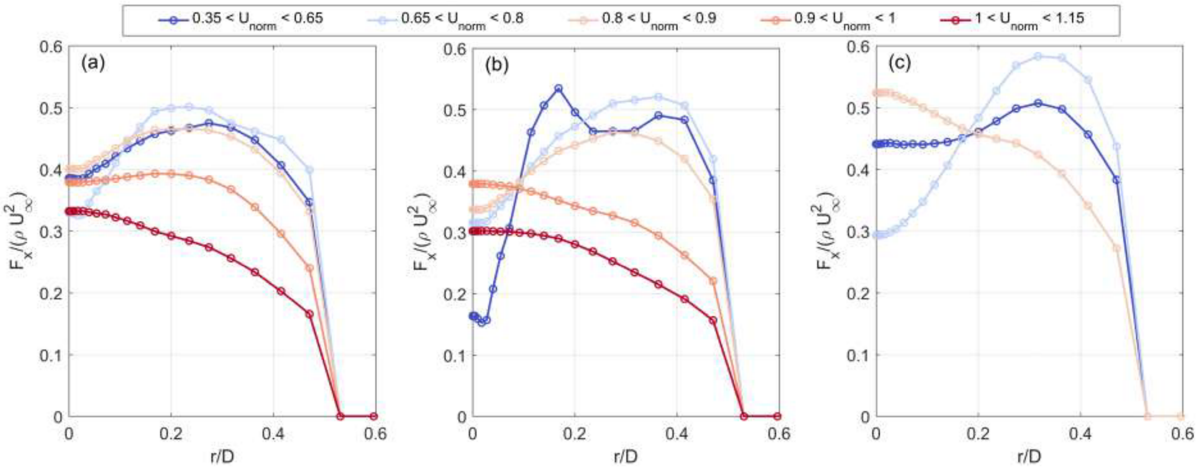

Figure 6. Distribution of local thrust along the blade span for different atmospheric stability regimes: a) stable; b) neutral; c) convective.

With increasing incoming wind speed, the reduction of the aerodynamic load due to the higher blade pitch angle is clearly detected. It is also observed that the major load reduction occurs in proximity of the blade tip. For a given incoming wind speed, the integral thrust force is generally increased by transitioning from stable, neutral to convective regimes. This feature is better highlighted through the thrust coefficient, C_t, reported in Fig. 7. C_t confirms the reduction of loading occurring for transition from region 2 to region 3. The C_t estimated through the proposed procedure, consisting in coupling RANS simulations and LiDAR data, is compared with estimates by only using LiDAR data or derived from the power measurements recorded by the SCADA. Only using SCADA data, the C_t is generally under-estimated, which is a consequence of neglecting the thrust connected with turbine tower, nacelle, or the blade stall for different wind conditions and positions along the blade span not being detected through the power measurements, while probed by the LiDAR. Furthermore, the procedure consisting in coupling LiDAR measurements and RANS simulations allows recovering the trend of an increased thrust coefficient and, thus, power coefficient observed by the SCADA data, which, in contrast, is not preserved when only using LiDAR data.

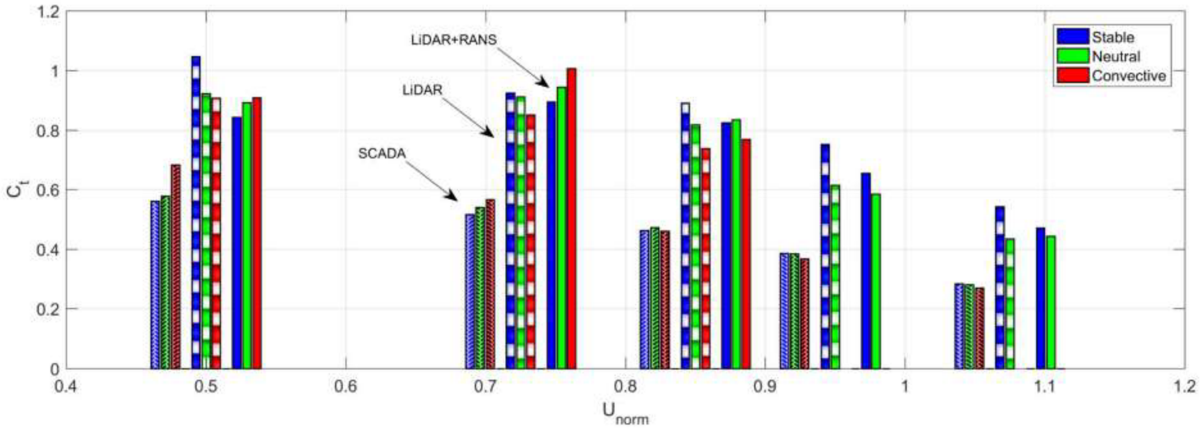

Figure 7. Thrust force coefficient, C_t, for each cluster estimated from SCADA data, LiDAR data and the iterative RANS-LiDAR procedure.

6. Concluding remarks

Ground-based LiDAR measurements of wakes generated by wind turbines at an onshore wind farm in Texas have been coupled with wake RANS simulations in order to quantify the axial induction of the wind turbines for different operative conditions of the rotors and atmospheric stability regime of the incoming wind.

The LiDAR wake measurements have been thoroughly post-processed in order to estimate the time-averaged wake velocity fields for different data clusters based on incoming wind speed and atmospheric stability condition. This data analysis has allowed removing from the wake measurements effects of the incoming atmospheric boundary layer profile, variability of mean wind direction and fluctuations due to meandering.

The rotor axial induction has been calculated through a control volume analysis of the axial momentum by leveraging the LiDAR measurements and the radial velocity, pressure and momentum fluxes estimated through the RANS simulations. This iterative procedure is arrested when differences between the LIDAR and RANS streamwise velocity fields are minimized.

The axial induction estimated by coupling LiDAR measurements and RANS simulations has allowed to detect the reduction of the thrust force over the turbine blades for increasing incoming wind speed when transitioning from region 2 to region 3 of the turbine power curve. A lower thrust force is generally observed for stable conditions with respect to neutral and convective conditions, which confirms results obtained from SCADA data.

The proposed procedure can be considered as an empirical data-driven alternative to the current actuator disk/line models in order to simulate wind turbine wakes with more realistic aerodynamic forcing of the turbine rotor for different operative conditions and regimes of the atmospheric stability. A limitation of the current approach is represented by the axisymmetric assumption used for the wakes, which is a consequence of the 2D LiDAR scans performed not allowing a 3D characterization of the wakes. This limitation can be overcome by using a 3D RANS solver and performing 2D measurements over vertical cross-planes upstream and in the wake of a turbine with faster continuous scanning LiDARs. An effect of this limitation might be the estimate of slightly larger wakes and over-estimated thrust under stable stability conditions, for which wakes are skewed and become less axisymmetric due to the presence of wind veer.

Acknowledgments

This work was supported by the NSF CBET grant 1705837, program manager Ronald Joslin. This material is based upon work supported by the National Science Foundation under Grant Number IIP-1362022 (Collaborative Research: I/UCRC for Wind Energy, Science, Technology, and Research) and from the WindSTAR I/UCRC Members: Aquanis, Inc., EDP Renewables,

Bachmann Electronic Corp., GE Energy, Huntsman, Hexion, Leeward Asset Management, LLC, Pattern Energy, and TPI Composites. Any opinions, findings, and conclusions or recommendations expressed in this material are those of the authors and do not necessarily reflect the views of the sponsors. Computational resources were provided by TACC.

References

[1] Santhanagopalan V, Rotea MA and Iungo GV 2018 Performance optimization of a wind turbine column for different incoming wind turbulence. *Renewable Energy* **116** pp 232-243.
[2] Santhanagopalan V, Letizia S, Zhan L, Al-Hamidi LY and Iungo GV 2018 Profitability optimization of a wind power plant performed through different optimization algorithms and a data-driven RANS solver. *AAIA SciTech, Wind Energy Symposium* AIAA 2018-2018.
[3] Iungo GV, Santhanagopalan V, Ciri U, Viola F, Zhan L, Rotea MA and Leonardi S 2018 Parabolic RANS solver for low-computational-cost simulations of wind turbine wakes. *Wind Energy* **21** pp 184-197.
[4] Iungo GV, Viola F, Ciri U, Leonardi S and Rotea MA 2016 Reduced order model for optimization of power production from a wind farm. *AAIA SciTech, Wind Energy Symposium* AIAA 2016-2200.
[5] Iungo GV, Viola F, Ciri U, Rotea MA and Leonardi S 2016 Data-driven RANS for simulations of large wind farms. *J. Phys.: Conf. Series* **625** 012025.
[6] Santoni C, Carrasquillo K, Arenas-Navarro I and Leonardi S 2017 Effect of tower and nacelle on the flow past a wind turbine. *Wind Energy* **20** (12) pp 1823-1839.
[7] Ciri U, Rotea MA, Santoni C and Leonardi S 2017 Large-eddy simulations with extremum-seeking control for individual wind turbine power optimization. *Wind Energy* **20** (9) pp 1617-1634.
[8] Jonkman J, Butterfield S, Musial W, Scott G 2009 Definition of a 5-MW reference wind turbine for offshore system development. *NREL Tech. Report.*
[9] El-Asha S, Zhan L, Iungo GV 2017 Quantification of power losses due to wind turbine wake interactions through SCADA, meteorological and wind LiDAR data. *Wind Energy* **11** pp 1823-1839.
[10] Sumner J and Masson C 2006 Influence of atmospheric stability on wind turbine power performance. *J. Solar Energy Eng.* **128** pp 531-538.
[11] St Martin CM, Lundquist JK, Clifton A, Poulos GS and Schreck SJ 2016 Wind turbine power production and annual energy production depend on atmospheric stability and turbulence. *Wind Energy Sci.* **1** pp 221-236.
[12] Iungo GV and Porté-Agel F 2014 Volumetric lidar scanning of wind turbine wakes under convective and neutral atmospheric stability regimes. *J. Atmos. Ocean. Technol.* **31** (10) pp 2035-2048.
[13] Abkar M and Porté-Agel F 2015 Influence of atmospheric stability on wind-turbine wakes: A large-eddy simulation study. *Phys. Fluids* **27** (3) 035104.
[14] Lundquist JK, Wilczak JM, Iungo GV et al. 2017 Assessing state-of-the-art capabilities for probing the atmospheric boundary layer: the XPIA field campaign. *Bullet. Amer. Meteorol. Soc.* **98** (2) pp 289-314.
[15] Debnath M, Iungo GV et al. 2017 Assessment of virtual towers performed with scanning wind lidars and Ka-band radars during the XPIA experiment. *Atmos. Meas. Tech.* **10** pp 1215-1227.
[16] Debnath M, Iungo GV et al. 2017 Vertical profiles of the 3-D wind velocity retrieved from multiple wind lidars performing triple range-height-indicator scans. *Atmos. Meas. Tech.* **10** (2) pp 431-444.
[17] Iungo GV 2016 Experimental characterization of wind turbine wakes: Wind tunnel tests and wind LiDAR measurements. *J. Wind Eng. Industr. Aerodyn.* **149** pp 35-39.
[18] Iungo GV and Porté-Agel F 2014 Volumetric scans of wind turbine wakes performed with three simultaneous wind LiDARs under different atmospheric stability regimes. *J. Phys.: Conf. Ser.* **524** (1) 0112164.
[19] Iungo GV and Porté-Agel F 2013 Measurement procedures for characterization of wind turbine wakes with scanning Doppler wind LiDARs. *Adv. Sci. Res.* **10** pp 71-75.
[20] Iungo GV, Wu Y-T and Porté-Agel F 2013 Field measurements of wind turbine wakes with lidars. *J. Atmos. Ocean. Technol.* **30** (2) pp 274-287.
[21] Carbajo-Fuertes F, Iungo GV and Porté-Agel F 2014 3D turbulence measurements using three synchronous wind lidars: validation against sonic anemometry. *J. Atmos. Ocean. Technol.* **31** (7) pp 1549-1556.
[22] Zhan L, Letizia S and Iungo GV 2018 LiDAR measurements for an onshore wind farm: wake variability for different incoming wind speed and atmospheric stability regime. Submitted to *Wind Energy.*
[23] Barnes SL 1964 A technique for maximizing details in numerical weather map analysis *J. Appl. Meteorol.* **2** pp 396-409.
[24] Madsen HA, Riziotis V, Zhale F, Hansen MOL, Snel H, Grasso F, Larsen TJ, Politis E and Rasmussen F 2012 Blade element momentum modeling of inflow with shear in comparison with advanced model results *Wind Energy* **15** pp 63-81.